Advances in computational methods for Quantum Field Theory calculations

Ruijl, B.J.G.

Author: Ruijl, B.J.G.
Title: Advances in computational methods for Quantum Field Theory calculations
Issue Date: 2017-11-02

4 RESULTS FOR FOUR-LOOP COMPUTATIONS

In this chapter we use the FORCER program, constructed in chapter 3 as part of the answer to **RQ2**, to compute two classes of four-loop objects. Class 1 concerns propagators and vertices of QCD, and Class 2 concerns Mellin moments of splitting functions and coefficient functions.

CLASS 1 The first class of objects that we are going to compute are the finite pieces of propagators and vertices to any power in $\epsilon = (D-4)/2$, where D is the space-time dimension. Up until this point, only the poles and the ε^0 coefficients are known, since they have been used in computations of the basic renormalisation group functions of QCD [23, 24, 113, 114, 119–126] which have recently reached five-loop accuracy [4, 40, 41, 127–129]. In the modified minimal subtraction ($\overline{\text{MS}}$) scheme [130, 131], defined by subtracting the poles in ε together with a fixed term that occurs in dimensional regularisation , these functions are obtained by computing single poles in corresponding Green's functions. Since only the poles are required, the above four- and five-loop results were first obtained using the method of infrared rearrangement [4, 124, 132–138] which simplifies computations without changing the ultraviolet singular structure, but modifies the finite parts. Therefore, it is not possible to compute the complete finite piece using these standard methods.

Our aim is to provide the self-energies and a set of vertices with one vanishing external momentum for massless QCD at four-loop accuracy. The unrenormalised results are exact in terms of ε, and four-loop master integrals [105, 106]. The computation has been performed for a general gauge group and in an arbitrary covariant linear gauge, by using the FORCER program [1, 7, 9] for massless four-loop propagator-type integrals. For the vertices, setting one of the momenta to zero effectively reduces vertex integrals to propagator-type integrals. In QCD this does not create Infrared (IR) divergences, which means the poles do not change. At the three-loop level, similar computations were performed in ref. [139], but with an expansion in ε. In addition, studies of QCD vertices in perturbation theory for various configurations include refs. [140–152].

We compute all QCD vertices in a general linear covariant gauge, with the exception of the four-gluon vertex for which there are at least three difficulties: first, two momenta have to be nullified before the diagrams become propagator-like. Second, the number of diagrams is large at four loops. Third, the colour structure for a generic group is no longer an overall factor, but will be term dependent.

A direct application of our results is to compute conversion factors for renormalisation group functions from the $\overline{\text{MS}}$ scheme to momentum subtraction schemes, see, e.g., refs. [140, 143]. In a later chapter (6.5), we will use the results presented here to convert the five loop beta function to the MiniMOM scheme [153]. The MiniMOM scheme is a momentum subtraction scheme that is more convenient than $\overline{\text{MS}}$ for comparing QCD in the perturbative and non-perturbative regime.

CLASS 2 The second class of objects we are going to compute are Mellin moments of four-loop splitting functions and coefficient functions. Even though for most cases three-loop accuracy is adequate, there are at least two cases where the next order is of interest due to (1) very high requirements on the theoretical accuracy, such as in the determination of the strong coupling constant α_s from deep-inelastic scattering (DIS), see, e.g., [154], or (2) a slow convergence of the perturbation series, such as for Higgs production in proton-proton collisions, see, e.g., [82, 155].

At present, a direct computation of the four-loop splitting functions appears to be too difficult. Work on low-integer Mellin moments of these functions started ten years ago [156]; until recently only the $N = 2$ and $N = 4$ moments had been obtained of the quark+antiquark non-singlet splitting function $P_{\rm ns}^{(3)+}$ together with the $N = 3$ result for its quark–antiquark counterpart $P_{\rm ns}^{(3)-}$ [157–159].

The goal in this chapter is to employ the FORCER program to extend the MINCER-based fixed Mellin-N calculations of refs. [84–86] to four-loop accuracy. We will use the optical theorem method [83–86] to compute low-N splitting functions and coefficient functions. Next, we will use the operator product expansion method [158, 160] to compute higher moments of splitting functions.

4

We now provide the layout of this chapter. In section 4.1, we define the group notations. In section 4.2, we compute Yang-Mills propagators and vertices with a vanishing momentum (objects of Class 1). Next, we compute Mellin moments of splitting functions and coefficient functions (objects of Class 2) in section 4.3. Finally, we provide the chapter conclusion in section 4.4.

4.1 GROUP NOTATIONS

In this section we will introduce our notations for the group invariants appearing in the remainder of this thesis. T^a are the generators of the representation of the fermions, and f^{abc} are the structure constants of the Lie algebra of a compact simple Lie group,

$$T^aT^b - T^bT^a \;=\; if^{abc}\,T^c\,. \tag{60}$$

The quadratic Casimir operators C_F and C_A of the N-dimensional fermion and the N_A-dimensional adjoint representation are given by $[T^aT^a]_{ik} \;=\; C_F\delta_{ik}$ and $f^{acd}f^{bcd} \;=\; C_A\delta^{ab}$, respectively. The trace normalisation of the fermion representation is $\text{Tr}(T^aT^b) \;=\; T_F\delta^{ab}$. At $L \geq 3$ loops also quartic group invariants enter the results. These can be expressed in terms of contractions of the totally symmetric tensors

$$\begin{aligned} d_F^{abcd} &= \frac{1}{6}\,\text{Tr}(T^a\,T^b\,T^c\,T^d \;+\; \text{five } bcd \text{ permutations }) \;, \\ d_A^{abcd} &= \frac{1}{6}\,\text{Tr}(C^aC^bC^cC^d \;+\; \text{five } bcd \text{ permutations }) \;. \end{aligned} \tag{61}$$

Here the matrices $[C^a]_{bc} = -if^{abc}$ are the generators of the adjoint representation. It should be noted that in QCD-like theories without particles that are colour neutral, Furry's theorem [161] prevents the occurrence of symmetric tensors with an odd number of indices.

For fermions transforming according to the fundamental representation and the standard normalisation of the SU(N) generators, these 'colour factors' have the values

$$
\begin{aligned}
T_F &= \frac{1}{2}, \quad C_A = N, \quad C_F = \frac{N_A}{2N} = \frac{N^2-1}{2N}, \quad \frac{d_A^{abcd}d_A^{abcd}}{N_A} = \frac{N^2(N^2+36)}{24}, \\
&\frac{d_F^{abcd}d_A^{abcd}}{N_A} = \frac{N(N^2+6)}{48}, \quad \frac{d_F^{abcd}d_F^{abcd}}{N_A} = \frac{N^4-6N^2+18}{96\,N^2}. \qquad (62)
\end{aligned}
$$

The results for QED (i.e., the group U(1)) are obtained for $C_A = 0$, $d_A^{abcd} = 0$, $C_F = 1$, $T_F = 1$, $d_F^{abcd} = 1$, and $N_A = 1$. For a discussion of other gauge groups the reader is referred to ref. [113].

4.2 PROPAGATORS AND VERTICES

In this section we will present the computation of four-loop QCD propagators and vertices with a vanishing momentum.

First, we summarise the notations for self-energies and vertex functions with one vanishing momentum presented in section 4.2.1 to section 4.2.4. In most cases we follow the conventions in ref. [139].[1] Next, we describe our renormalisation method in section 4.2.5 and how to compute anomalous dimensions in section 4.2.6. Finally, we present the results of our computation in section 4.2.7.

4.2.1 *Self energies*

The gluon, ghost and quark self-energies (figure 25) are of the form

$$\Pi^{ab}_{\mu\nu}(q) = -\delta^{ab}(q^2 g_{\mu\nu} - q_\mu q_\nu)\Pi(q^2), \qquad (63)$$

$$\tilde{\Pi}^{ab}(q) = \delta^{ab} q^2 \tilde{\Pi}(q^2), \qquad (64)$$

$$\Sigma^{ij}(q) = \delta^{ij} \not{q}\, \Sigma_V(q^2). \qquad (65)$$

The colour indices are understood such that a and b are for the adjoint representation of the gauge group, i and j for the representation to which the quarks transform. In eq. (63) we have used the fact that the Ward identities render the gluon propagator transversal. The 'form factors' $\Pi(q^2)$, $\tilde{\Pi}(q^2)$ and $\Sigma_V(q^2)$ can easily be extracted from contributions of the corresponding one-particle irreducible diagrams by applying

1 We note that these conventions may be different from the ones commonly used in the literature. In fact, the Feynman rules in FORCER are different as well, and hence we occasionally had to convert intermediate results from one convention to the other and back.

4

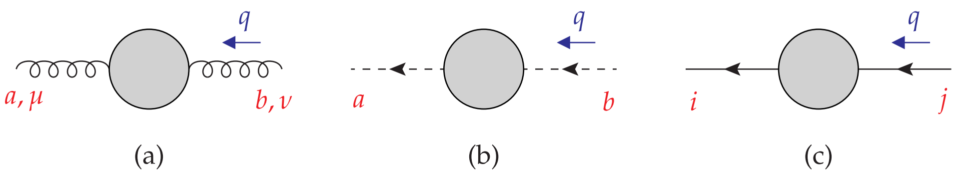

Figure 25: The gluon, ghost and quark self-energies $\Pi^{ab}_{\mu\nu}(q)$ (a), $\tilde{\Pi}^{ab}(q)$ (b) and $\Sigma^{ij}(q)$ (c).

projection operators [139] (the same holds for the vertex functions discussed below). They are related to the full gluon, ghost and quark propagators as follows:

$$D^{ab}_{\mu\nu}(q) = \frac{\delta^{ab}}{-q^2}\left[\left(-g_{\mu\nu} + \frac{q_\mu q_\nu}{q^2}\right)\frac{1}{1+\Pi(q^2)} - \xi\,\frac{q_\mu q_\nu}{q^2}\right], \tag{66}$$

$$\Delta^{ab}(q) = \frac{\delta^{ab}}{-q^2}\,\frac{1}{1+\tilde{\Pi}(q^2)}, \tag{67}$$

$$S^{ij}(q) = \frac{\delta^{ij}}{-q^2}\,\frac{\not{q}}{1+\Sigma_V(q^2)}. \tag{68}$$

Here the Landau gauge corresponds to $\xi = 0$, and the Feynman gauge to $\xi = 1$. We note that this convention differs from that in the widely used Form version [33] of the Mincer program [32] for three-loop self-energies, where the symbol `xi` represents $1-\xi$.

4

4.2.2 *Triple-gluon vertex*

Without loss of generality, one can set the momentum of the third gluon to zero, as depicted in figure 26. Then the triple-gluon vertex can be written in the following form:

$$\Gamma^{abc}_{\mu\nu\rho}(q,-q,0) = -igf^{abc}\left[(2g_{\mu\nu}q_\rho - g_{\mu\rho}q_\nu - g_{\rho\nu}q_\mu)\,T_1(q^2) - \left(g_{\mu\nu} - \frac{q_\mu q_\nu}{q^2}\right)q_\rho T_2(q^2)\right], \tag{69}$$

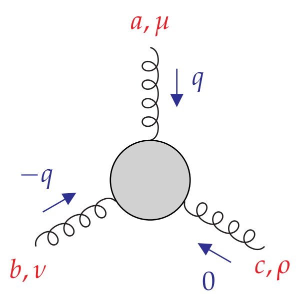

Figure 26: The triple-gluon vertex with one vanishing momentum, $\Gamma^{abc}_{\mu\nu\rho}(q,-q,0)$.

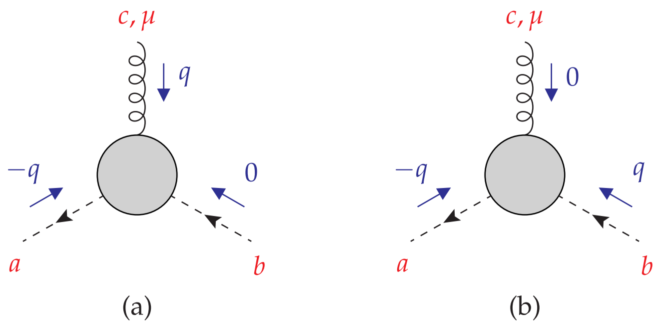

Figure 27: The ghost-gluon vertex: (a) $\tilde{\Gamma}^{abc}_{\mu}(-q,0;q)$ has a vanishing incoming ghost momentum and (b) $\tilde{\Gamma}^{abc}_{\mu}(-q,q;0)$ a vanishing gluon momentum.

where g is the coupling constant and f^{abc} are the structure constants of the gauge group in eq. 60. The first term in the square bracket corresponds to the tree-level vertex while the second term arises from radiative corrections, i.e., at the tree-level the form factors $T_{1,2}(q^2)$ read

$$T_1(q^2)\big|_{\text{tree}} = 1, \qquad T_2(q^2)\big|_{\text{tree}} = 0. \tag{70}$$

Because of Furry's theorem [161] and the fact that we have no colour-neutral particles, symmetric invariants with an odd number of indices cannot occur for internal fermion lines. Neither can such invariants occur for the adjoint representation. Hence, if we project out a d^{abc} structure, we would get a scalar invariant with an odd number of f tensors, and such a combination must be zero. This has been checked explicitly to the equivalent of six-loop vertices in ref [112]. Due to the bosonic property of gluons, the totally antisymmetric colour factor f^{abc} leads to antisymmetric Lorentz structure as in eq. (69). One could consider another Lorentz structure,

$$-igf^{abc}q_\mu q_\nu q_\rho T_3(q^2). \tag{71}$$

However, a Slavnov-Taylor identity requires $T_3(q^2)$ to vanish [139].

4.2.3 *Ghost-gluon vertex*

Since the tree-level vertex is proportional to the outgoing ghost momentum in our convention, nullifying this momentum gives identically zero in perturbation theory. Therefore, we only have two possibilities to set one of the external momenta to zero. One is the incoming ghost momentum and the other is the gluon momentum (figure 27):

$$\tilde{\Gamma}^{abc}_{\mu}(-q,0;q) = -igf^{abc}q_\mu\tilde{\Gamma}_h(q^2), \tag{72}$$

$$\tilde{\Gamma}^{abc}_{\mu}(-q,q;0) = -igf^{abc}q_\mu\tilde{\Gamma}_g(q^2). \tag{73}$$

4

The subscript h of $\tilde{\Gamma}_h(q^2)$ indicates the function with vanishing incoming ghost momentum, whereas g of $\tilde{\Gamma}_g(q^2)$ denotes the vanishing gluon momentum. These functions are equal to one at the tree-level,

$$\tilde{\Gamma}_h(q^2)\big|_{\text{tree}} = \tilde{\Gamma}_g(q^2)\big|_{\text{tree}} = 1. \tag{74}$$

4.2.4 *Quark-gluon vertex*

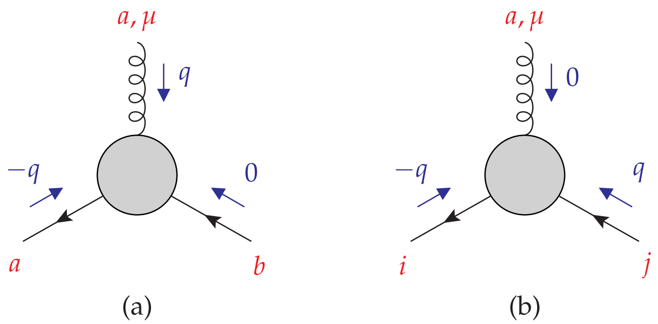

Figure 28: The quark-gluon vertex: (a) $\Lambda^a_{\mu,ij}(-q,0;q)$ has a vanishing incoming quark momentum and (b) $\Lambda^a_{\mu,ij}(-q,q;0)$ a vanishing gluon momentum.

We consider the case of a vanishing incoming quark momentum and the case of a vanishing gluon momentum (figure 28). Nullifying the outgoing quark momentum gives the same result as nullifying the incoming quark momentum. Then the vertex can be written as

$$\Lambda^a_{\mu,ij}(-q,0;q) = gT^a_{ij}\Big[\gamma_\mu \Lambda_q(q^2) + \gamma^\nu\Big(g_{\mu\nu} - \frac{q_\mu q_\nu}{q^2}\Big)\Lambda^T_q(q^2)\Big], \tag{75}$$

$$\Lambda^a_{\mu,ij}(-q,q;0) = gT^a_{ij}\Big[\gamma_\mu \Lambda_g(q^2) + \gamma^\nu\Big(g_{\mu\nu} - \frac{q_\mu q_\nu}{q^2}\Big)\Lambda^T_g(q^2)\Big]. \tag{76}$$

T^a_{ij} are the generators of the representation for the quarks. The subscript q indicates the functions with vanishing incoming quark momentum and g indicates those with vanishing gluon momentum. At the tree-level we have

$$\Lambda_q(q^2)\big|_{\text{tree}} = \Lambda_g(q^2)\big|_{\text{tree}} = 1, \tag{77}$$

$$\Lambda^T_q(q^2)\big|_{\text{tree}} = \Lambda^T_g(q^2)\big|_{\text{tree}} = 0. \tag{78}$$

4.2.5 *Renormalisation*

All the quantities we compute contain divergences. The theory of renormalisation states that for QCD these can be absorbed into redefinitions of the interaction strength, mass parameter, and field definitions. This implies that the observables such as the mass of a particle, and the strength of the strong coupling constant depend on the energy scale at which one measures. In this section we will define renormalisation constants which make the observable quantities finite.

In a generic renormalisation scheme R, the respective renormalisations of the gluon, ghost and quark fields can be written as

$$(A^B)^a_\mu = \sqrt{Z_3^R}\,(A^R)^a_\mu, \tag{79}$$

$$(\eta^B)^a = \sqrt{\tilde{Z}_3^R}\,(\eta^R)^a, \tag{80}$$

$$\psi^B_{if} = \sqrt{Z_2^R}\,\psi^R_{if}. \tag{81}$$

The superscript "B" indicates a bare (divergent) quantity and "R" a renormalised (finite) one. For the coupling constant, we define $a = \alpha_s/(4\pi) = g^2/(16\pi^2)$. Then a and the gauge parameter ξ are renormalised in dimensional regularisation ($D = 4 - 2\varepsilon$) as follows:

$$a^B = \mu^{2\varepsilon} Z_a^R a^R, \tag{82}$$

$$\xi^B = Z_3^R \xi^R. \tag{83}$$

Here μ is the 't Hooft mass scale, which is added to make the coupling constant dimensionless. We have used the fact that the gauge parameter is also renormalised by the gluon field renormalisation constant, $Z_\xi^R = Z_3^R$. The renormalisation of the self-energies and vertex functions is performed as

4

$$1 + \Pi^R = Z_3^R(1 + \Pi^B), \tag{84}$$

$$1 + \tilde{\Pi}^R = \tilde{Z}_3^R(1 + \tilde{\Pi}^B), \tag{85}$$

$$1 + \Sigma_V^R = Z_2^R(1 + \Sigma_V^B), \tag{86}$$

and

$$T_i^R = Z_1^R T_i^B, \qquad i = 1, 2, \tag{87}$$

$$\tilde{\Gamma}_i^R = \tilde{Z}_1^R \tilde{\Gamma}_i^B, \qquad i = h, g, \tag{88}$$

$$\Lambda_i^R = \bar{Z}_1^R \Lambda_i^B, \qquad \Lambda_i^{T,R} = \bar{Z}_1^R \Lambda_i^{T,B}, \qquad i = q, g, \tag{89}$$

where the vertex renormalisation constants are related to the field and coupling renormalisation constants via the Slavnov-Taylor identities by

$$\sqrt{Z_a^R Z_3^R} = \frac{Z_1^R}{Z_3^R} = \frac{\tilde{Z}_1^R}{\tilde{Z}_3^R} = \frac{\bar{Z}_1^R}{Z_2^R}. \tag{90}$$

In MS-like schemes, the renormalisation constants contain only pole terms with respect to ε and thus take the form

$$Z_i^{\mathrm{MS}} = 1 + \sum_{l=1}^{\infty} a^l Z_i^{\mathrm{MS},(l)} = 1 + \sum_{l=1}^{\infty} a^l \sum_{n=1}^{l} \frac{Z_i^{\mathrm{MS},(l,n)}}{\varepsilon^n}. \tag{91}$$

The coefficients $Z_i^{\text{MS},(l,n)}$ are determined order by order in such a way that any renormalised Green's function becomes finite. Below we give an example for the three-loop background field propagator G. In the background field the field strength renormalisation is simply $Z_a^{-1/2}$ (see section 6.2). We assume we are in the Landau gauge ($\xi = 0$), so that we need not worry about renormalising ξ:

$$\begin{aligned} G_B &= 1 + a_B G_1 + a_B^2 G_2 + a_B^3 G_3 + \dots\ , \\ G_R &= Z_a^{-1}(1 + aZ_a G_1 + a^2 Z_a^2 G_2 + a^3 Z_a^3 G_3 + \dots) \\ &= 1 + a(G_1 - Z^{\text{MS},(1)}) + a^2(G_2 + Z^{\text{MS},(1)^2} - Z^{\text{MS},(2)}) \\ &\quad + a^3(G_3 + G_2 Z^{\text{MS},(1)} - Z^{\text{MS},(1)^3} + 2Z^{\text{MS},(1)} Z^{\text{MS},(2)} - Z^{\text{MS},(3)}) + \dots\ . \end{aligned} \tag{92}$$

If we introduce the pole operator $K(\sum_{i=-\infty}^{\infty} \frac{x_i}{\varepsilon^i}) = \sum_{i=-\infty}^{-1} \frac{x_i}{\varepsilon^i})$, which takes the pole part of a Laurent series in ε, we can write:

$$\begin{aligned} Z^{\text{MS},(1)} &= K(G_1)\ , \\ Z^{\text{MS},(2)} &= K(G_2) + K(G_1)^2\ , \\ Z^{\text{MS},(3)} &= K(G_3) + K\left(G_2 K(G_1)\right) - K(G_1)^3 + 2K(G_1)\left(K(G_2) + K(G_1)^2\right)\ . \end{aligned} \tag{93}$$

In the case of computing other self-energies, the field strength renormalisation will not be $Z_a^{-1/2}$, but will have its own Z. This means a system of equations has to be solved. For perturbatively renormalisable theories, such a system can always be solved order by order.

4.2.6 *Anomalous dimensions*

Renormalisation introduces an arbitrary scale μ on which the bare quantities do not depend. Let us take for example the gluon propagator with zero quark masses $R(Q, a, \xi, \mu) = Z_3 R_B(Q, Z_a a_B, Z_3 \xi_B)$, where we suppress the MS label and we have used the fact that gauge invariance ensures that the gauge parameter is renormalised with Z_3. If we enforce that $\frac{dR_B}{d\mu} = 0$ we obtain the following Callan-Symanzik renormalisation group equation [162, 163]:

$$\begin{aligned} \mu^2 \frac{d}{d\mu^2} R(Q, a) &= \left[\mu^2 \frac{\partial}{\partial \mu^2} + \mu^2 \frac{da}{d\mu^2} \frac{\partial}{\partial a} + \mu^2 \xi \frac{d \ln \xi}{d\mu^2} \frac{\partial}{\partial \xi} - \mu^2 \frac{d \ln Z_3}{d\mu^2}\right] R(Q, a) \\ &\equiv \left[\mu^2 \frac{\partial}{\partial \mu^2} + \tilde{\beta} \frac{\partial}{\partial a} + \xi \gamma_3 \frac{\partial}{d\xi} - \gamma_3\right] R(Q, a) = 0\ , \end{aligned} \tag{94}$$

where the quantity γ_3 is the anomalous dimension of the external gluon field and $\tilde{\beta}$ is the D-dimensional beta function. The anomalous dimension γ_3 describes how the field evolves with the energy scale, and $\tilde{\beta}$ describes how the strong coupling constant evolves with the energy scale.

We rewrite:

$$\begin{aligned}\tilde{\beta} &\equiv \mu^2 \frac{da}{d\mu^2} = \mu^2 \frac{dZ_a^{-1} a_B}{d\mu^2} \\ &= \mu^2 Z_a^{-1} \frac{da_B}{d\mu^2} + \mu^2 a_B \frac{dZ_a^{-1}}{d\mu^2} \\ &= -\varepsilon a + \mu^2 a Z_a^{-1} \frac{dZ_a}{da} \frac{da}{d\mu^2} \\ &= -\varepsilon a + a \frac{d \ln Z}{da} \tilde{\beta} \\ &\equiv -\varepsilon a + \beta \,,\end{aligned} \tag{95}$$

where β is the beta function in four dimensions and we used that the beta function is gauge independent in MS-like schemes.

For both the beta function and anomalous dimension, the following reasoning holds (where γ is the anomalous dimension associated with Z):

$$\begin{aligned}Z\gamma = Z\mu^2 \frac{d \ln Z}{d\mu^2} &= \mu^2 \frac{\partial Z}{\partial a} \frac{da}{d\mu^2} + \mu^2 \frac{\partial Z}{\partial \xi} \frac{d\xi}{d\mu^2} \\ &= \frac{\partial Z}{\partial a}(-\varepsilon a + \beta) + \frac{\partial Z}{\partial \xi} \gamma_3,\end{aligned} \tag{96}$$

This equation holds for any power of ε, so we compare the ε^0 part (for which β and γ_3 drop out):

$$\gamma = -\sum_{n=1}^{\infty} n a^n Z^{\mathrm{MS},(n,1)}, \qquad \beta = -\sum_{n=1}^{\infty} n a^n Z_a^{\mathrm{MS},(n,1)} \,. \tag{97}$$

Even though the anomalous dimensions are thus only comprised of the simple poles of Z in MS-like renormalisation schemes, there is no loss of information: the entire Z can be reconstructed from (96). This also means that the higher-order poles of Z are completely determined by lower-order renormalisation group contributions. Consequently, the higher-order poles serve as a check for higher-order results.

4.2.7 *Computations and checks*

The results in this section are obtained by direct computation using the Forcer package, as described in chapter 3. The topologies are mapped to a built-in Forcer topology, after nullifying a leg for the vertices. To extract the form factors defined above, a generalisation of the projection operators in ref. [139] to a generic gauge group is used. Then the Feynman rules are applied. The remaining Lorentz-scalar integrals (which include loop-momenta numerators) are computed by the Forcer program.

The computation time varied between an hour and a week, on a single computer. The easy cases, such as the ghost propagator and quark propagator took an hour.

4

The gluon propagators and ghost-gluon-gluon vertex and quark-gluon-gluon vertex took about eight hours per configuration. The triple gluon vertex was the hardest case and took a week per configuration on a single machine with 24 cores. Had we chosen to compute with an expansion in ε, the computations would have been much faster.

We have checked our setup and results in various ways.

- The longitudinal component of the gluon self-energy $\delta^{ab} q_\mu q_\nu \Pi_L(q^2)$, see eq. (63), was shown to be zero by an explicit calculation at the four-loop level.
- The form factor $T_3(q^2)$ of the triple-gluon vertex in eq. (71) was computed and indeed vanished at the four-loop level.
- All the self-energies and vertex functions computed in this work were compared up to three loops with those in ref. [139]. Note that the finite parts of the vertex-function results in ref. [139] are only correct for SU(N) gauge groups, since the presence of quartic Casimir operators was not taken into account in the reconstruction of the general case. This fact was also noted in ref. [129].
- The four-loop renormalisation constants and anomalous dimensions for the case of SU(N) and a general linear covariant gauge were provided in ancillary files of ref. [126]. Directly after Forcer was completed, we established agreement with those results. For a generic group our results are in agreement with ancillary files of ref. [129].
- We remark that the ghost-gluon vertex is unrenormalised $\tilde{Z}_1^{\overline{\mathrm{MS}}} = \tilde{Z}_3^{\overline{\mathrm{MS}}} \sqrt{Z_a^{\overline{\mathrm{MS}}} Z_3^{\overline{\mathrm{MS}}}}$ $= 1$ in the Landau gauge. Moreover, our results confirm that the vertex has no radiative corrections when the incoming ghost momentum is nullified (i.e., $\tilde{\Gamma}_h^{\overline{\mathrm{MS}}} = 1$) in the Landau gauge up to four loops.

Since the results are rather lengthy, we will not include them in this thesis. All result can be obtained in a digital form as ancillary files to the article [2]. The files contain the bare results for the self-energies and vertices in terms of master integrals with coefficients that are exact in for any dimension D, as well as the results in the $\overline{\mathrm{MS}}$ scheme for $D = 4$.

4.3 SPLITTING FUNCTIONS AND COEFFICIENT FUNCTIONS

In order to describe collisions involving protons in colliders, one effectively describes the interactions between a particle from a proton, called a parton, and a probe. The probe could be a parton or any of the force carriers. The interaction depends on the relative momenta of the particles, their energy, and their type (up quark, down quark, gluon, etc). Consequently, an accurate model of the proton structure is required. A critical ingredient is the *parton density function* (pdf), which captures the probability that a certain particle with a certain (collinear) momentum fraction is inside the proton. A pdf has to be experimentally determined, since it involves low-energy

QCD which is outside the regime of perturbation theory. It also depends on the renormalisation scale, and this dependence can be determined by making precise computations in perturbative QCD.

Since QFT predicts that particles can briefly split up into others (for example a quark splitting into a quark with smaller momentum and a gluon), quantum corrections will influence the pdfs. How sensitive the system is to these virtual particles depends on the energy at which we are measuring. Below we show the DGLAP equation [164–166], which describes the dependence of a pdf f_i for a parton i (could be all light quarks, light antiquarks and the gluon), depending on an energy scale μ^2 (we set the factorisation scale to the renormalisation scale without loss of generality):

$$\frac{\partial f_i(x,\mu^2)}{\partial \mu^2} = \frac{\alpha_s(\mu^2)}{2\pi} \int_x^1 \frac{dz}{z} \left[\sum_j f_j(z,\mu^2) P_{ij}\left(\frac{x}{z}, \alpha_s(\mu^2)\right) \right] \tag{98}$$

where x is the fraction of the proton momentum, j sums over all possible partons, the integral is over all possible momentum fractions, and P_{ij} are the *splitting functions*: a quantity related to the probability that parton j will split up into i and other particles. What this equation in essence describes is that the probability of finding a parton i with momentum fraction x is changed by the event where a parton with a higher energy splits up into a parton of type i with exactly momentum fraction x.

Equation (98) is a complicated integro-differential equation. To solve it, we first turn the convolution of the splitting function and the pdf in eq. (98) into an ordinary product using a Mellin transform:

4

$$f_i(N,\mu^2) = \int_0^1 dx\, x^{N-1} f_i(x,\mu^2)\,. \tag{99}$$

The Mellin moments of splitting functions can be decoupled into a $2n_f - 1$ scalar equations and a 2x2 flavour-singlet system, see, e.g., [5, 8]. The non-singlet splitting functions $P^{\pm}_{\text{ns}}$ are the two combinations of quark–quark and quark–anti-quark splitting functions relevant to the $2n_f - 2$ flavour differences

$$q^{\pm}_{\text{ns},ik} = q_i \pm \bar{q}_i - (q_k \pm \bar{q}_k) \tag{100}$$

of quark distributions that evolve as scalars [167].

Since even or odd Mellin moments of splitting functions are anomalous dimensions, they are often expressed as such. We are going to calculate them up to fourth order in the reduced coupling constant $a = a_s/4\pi$:

$$\gamma^{\pm}_{\text{ns}}(N) = -P^{\pm}_{\text{ns}}(N) = -aP^{\pm(0)}_{\text{ns}}(N) - a^2 P^{\pm(1)}_{\text{ns}}(N) - a^3 P^{\pm(2)}_{\text{ns}}(N) - a^4 P^{\pm(3)}_{\text{ns}}(N)\,. \tag{101}$$

We will discuss two different methods to compute Mellin moments of splitting functions. The first is the optical theorem method described in section 4.3.1, and the second is the operator method described in section 4.3.2. Finally, we compute the axial vector current in 4.3.3.

4.3.1 *Optical theorem method*

The higher Mellin moments N can be obtained for the splitting functions $P_{ij}(N)$, the better an approximation can be made for the splitting functions in x-space. We use exactly the same method as described in [83–86], only we use Forcer instead of Mincer. In summary, using the optical theorem and a dispersion relation, the bare structure functions can be expressed as forward amplitudes. After applying a harmonic projection to isolate the desired coefficient, the Mellin moment of the structure function is expressed in terms of a propagator integral. These integrals are then computed with Forcer. The $1/\varepsilon$ poles provide the splitting functions. The finite piece after renormalisation yields the coefficient function.

Using this procedure, we have computed up to $N = 6$ for the non-singlet splitting functions and coefficient functions [8]. In figure 29 we show the results for the first Mellin moments. The dashed and dotted lines are the Padé approximations from the three-loop results of ref. [34]. For the singlet case, we have computed up to $N = 4$.

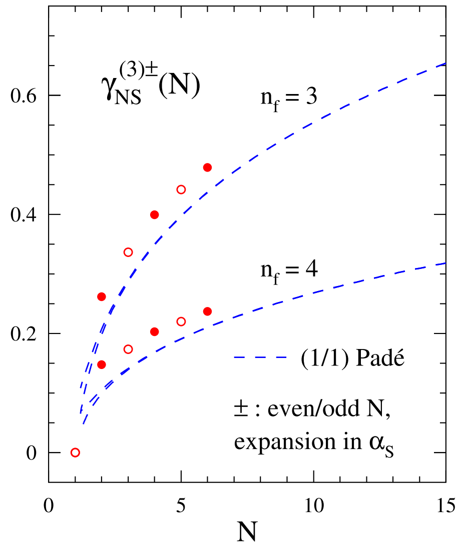

Figure 29: The lowest three even-N and odd-N values, respectively, of the anomalous dimensions $\gamma_{\mathrm{NS}}^{(3)+}$ and $\gamma_{\mathrm{NS}}^{(3)-}$, compared to Padé estimates derived from the NNLO results of ref. [34].

We have computed significantly more moments for specific colour factors. For diagrams with a high number of (light) fermion loops, indicated by powers of n_f, the complexity of the diagrams is simplified: for P_{qq} there are no four-loop diagrams without insertions that have a fermion loop. In figure 30 we show *all* three-loop graphs with two fermion loops, where a single fermion insertion on one of the gluon lines is understood. These graphs have been evaluated to the 40th Mellin moment, leading to more than complexity 80 integrals (as defined in section 3.5).

This provided enough information to reconstruct the analytic form in N using the LLL-algorithm [88, 168]. With this method, we have computed the n_f^2 contribution for the four-loop non-singlet splitting function and the n_f^3 contribution to the four-loop singlet splitting function [5].

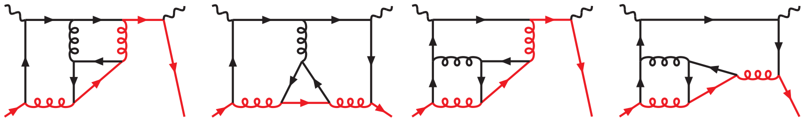

Figure 30: All three-loop diagrams with n_f^2 for P_{qq}, where a single fermion insertion on one of the gluon propagators is understood. There are no four-loop diagrams of this kind.

4.3.2 *Operator method*

Another way to compute moments of splitting functions is the light-cone operator product expansion (OPE) method [158, 160]. Although there are some challenges in constructing the operators, the advantage is that the complexity of the integrals scales like N, whereas for the optical theorem method it scales like $2N$. The coefficient functions are not addressed in this approach.

We have computed the non-singlet splitting function up to $N = 16$ moments [115]. In the large-n_c limit, up to $N = 19$ has been computed. Eighteen moment were used for a full reconstruction of the N dependence, and the nineteenth was used to confirm the result. Since in the large-n_c limit, $\gamma_{\mathrm{NS}}^{-} = \gamma_{\mathrm{NS}}^{+}$, both even and odd moments could be used in the reconstruction.

In figure 31 we show how the large-n_c limit matches up with the first 16 moments of the non-singlet splitting function, when studying the n_f^0 and n_f^1 coefficient. We expect an error of about 10% percent ($\frac{n_c}{n_c^3}$) for QCD that will decrease at large N. We see that even for low N, the error is less than 10% and that the (relative) error decreases fast with high N.

In figure 32 we show how moments of the non-singlet splitting function compare to the large-n_c result, for physical values of n_f. For $n_f = 3, n_f = 4$, and $n_f = 6$, we see that the error is small, even for low values of N. For the physically important $n_f = 5$, sizeable cancellations between non-n_f and n_f pieces result in a loss of accuracy for the large-n_c limit. To improve the large-n_c approximation, some (approximations of) non-leading large-n_c contributions have to be computed as well.

Since we have reconstructed the non-singlet splitting function for all N, we can study the large-N behaviour. It has the following form in $\overline{\mathrm{MS}}$ [169–171]:

$$\gamma = A \ln N + B + C \frac{1}{N} \ln N + D \frac{1}{N} + \dots \qquad (102)$$

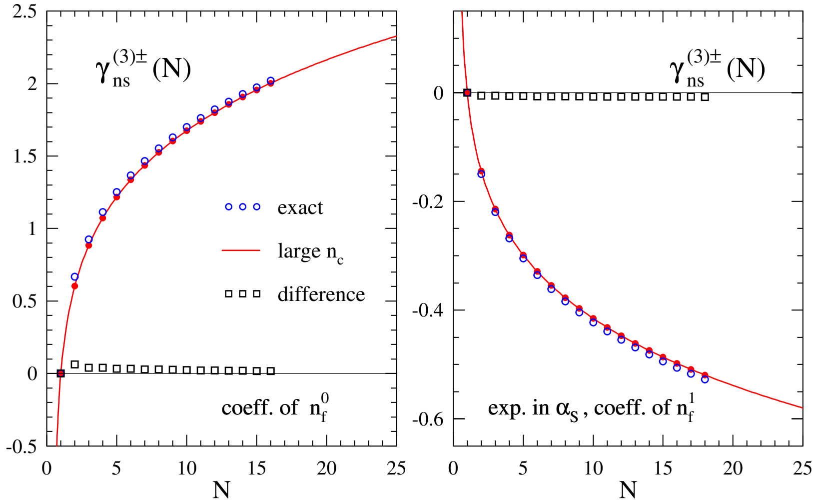

Figure 31: The large n_c limit versus the first Mellin moments of the non-singlet splitting function. The error is small, even for low N.

where A is a quantity known as the cusp anomalous dimension. This quantity is relevant beyond pdf evolution and is for example used in soft-gluon exponentiation and soft-collinear effective theories (SCET).

Taking the limit of $N \to \infty$ on our result yields a new $n_c^3 C_F$ term for the four-loop cusp anomalous dimension:

$$\gamma_{\text{cusp}}^{(3)} = + n_c^3 C_F \left(+ \frac{84278}{81} - \frac{88832}{81}\zeta_2 + \frac{20992}{27}\zeta_3 + 1804\zeta_4 - \frac{352}{3}\zeta_3\zeta_2 \right. \\ \left. - 352\zeta_5 - 32\zeta_3^2 - 876\zeta_6 \right) + \dots .$$

The $n_c^3 C_F$ term was soon afterwards confirmed via a calculation of the γqq form factor in the large-n_c limit [172].

4.3.3 *Axial vector current*

In order to compute the vector-axial interference structure function F_3, it is necessary to know the anomalous dimension of the axial vector current $\gamma^\mu \gamma^5$ to correct the treatment of γ_5. This can be retrieved from the ratio of the vector current (quark-quark-photon vertex) and axial vector current (quark-quark-Z vertex). The quark-quark-Z current contains a γ^5, which in its standard description as $i\gamma_0\gamma_1\gamma_2\gamma_3$ is strictly 4-dimensional instead of D-dimensional. To work around this issue we use

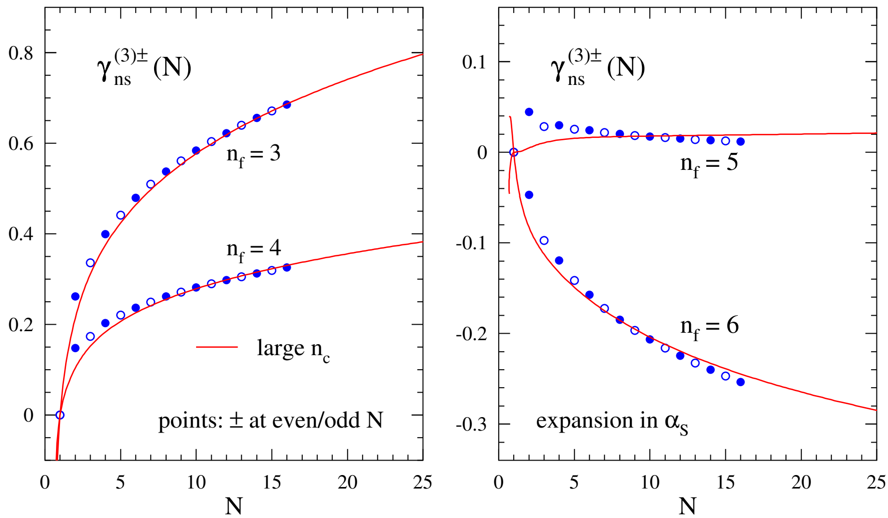

Figure 32: Comparison of the large n_c limit to Mellin moments of the non-singlet splitting functions for physical values of n_f.

the so-called Larin prescription of [173, 174]: $\gamma^\mu\gamma^5 = i\epsilon_{\mu\nu\rho\sigma}\gamma^\nu\gamma^\rho\gamma^\sigma$. As a projector, we use:

$$P = \frac{\epsilon_{\mu\nu\rho\sigma}\gamma^\nu\gamma^\rho\gamma^\sigma}{4(D-1)(D-2)(D-3)}\,, \tag{103}$$

which makes the tree-level contribution 1.

However, the Larin prescription breaks the axial Ward identity [173, 174]. As a result, an additional renormalisation for the axial vector current relative to the vector current is required. We define two quantities: Z_A and Z_5. Z_A is the additional renormalisation required for the axial current, and Z_5 is an extra finite renormalisation. Z_5 is used to map the renormalised axial current onto the renormalised vector current to 'fix' the anomaly. Given the renormalisation of the vector current V and the axial current A:

$$V_R = Z_{VC}V_B\,, \qquad A_R = Z_{AC}A_B\,, \tag{104}$$

where Z_{VC} and Z_{AC} contain the quark field renormalisation Z_2, the renormalisation of the strong coupling Z_a, and the renormalisation of the gauge parameter Z_3.

From these quantities, we can compute Z_A and Z_5:

$$Z_A = \frac{Z_{AC}}{Z_{VC}}\,, \qquad Z_5 = \lim_{\epsilon\to 0}\frac{V_R}{A_R}\,. \tag{105}$$

Both Z_A and Z_5 are gauge invariant. We have checked this by running with all powers of the gauge parameter.

Calculating the traces is the most expensive part of the computation. Using the optimisation from [175], we could have made the calculation much faster. The total computation takes 107 hours to compute on a single 2.4 GHz core. Below we present the results.

$$
\begin{aligned}
Z_A^{(2)} &= \frac{1}{\epsilon}\left(\frac{22}{3}C_AC_F - \frac{8}{3}C_FT_Fn_f\right),\\
Z_A^{(3)} &= \frac{1}{\epsilon^2}\left(\frac{3578}{81}{C_A}^2C_F - \frac{308}{9}C_A{C_F}^2 - \frac{1664}{81}C_AC_FT_Fn_f + \frac{64}{9}{C_F}^2T_Fn_f + \frac{32}{81}C_F{T_F}^2{n_f}^2\right)\\
&\quad + \frac{1}{\epsilon}\left(-\frac{484}{27}{C_A}^2C_F + \frac{352}{27}C_AC_FT_Fn_f - \frac{64}{27}C_F{T_F}^2{n_f}^2\right),\\
Z_A^{(4)} &= \frac{1}{\epsilon^3}\Bigg[{C_A}^3C_F\left(\frac{36607}{108} - 154\zeta_3\right) + {C_A}^2{C_F}^2\left(-\frac{29309}{54} + 440\zeta_3\right) + C_A{C_F}^3\left(\frac{935}{6}\right.\\
&\quad \left. - 264\zeta_3\right) + {C_A}^2C_FT_Fn_f\left(-\frac{16058}{81} - \frac{8}{3}\zeta_3\right) + C_A{C_F}^2T_Fn_f\left(\frac{4762}{27} - \frac{304}{3}\zeta_3\right)\\
&\quad + {C_F}^3T_Fn_f\left(-\frac{80}{3} + 96\zeta_3\right) + C_AC_F{T_F}^2{n_f}^2\left(\frac{734}{81} + \frac{64}{3}\zeta_3\right) + {C_F}^2{T_F}^2{n_f}^2\left(\frac{80}{27}\right.\\
&\quad \left. - \frac{64}{3}\zeta_3\right) + \frac{208}{81}C_F{T_F}^3{n_f}^3\Bigg] + \frac{1}{\epsilon^2}\left(-\frac{26411}{162}{C_A}^3C_F + \frac{605}{9}{C_A}^2{C_F}^2\right.\\
&\quad + \frac{1262}{9}{C_A}^2C_FT_Fn_f - \frac{176}{9}C_A{C_F}^2T_Fn_f - \frac{824}{27}C_AC_F{T_F}^2{n_f}^2 - \frac{16}{9}{C_F}^2{T_F}^2{n_f}^2\\
&\quad \left. + \frac{32}{81}C_F{T_F}^3{n_f}^3\right) + \frac{1}{\epsilon}\left(\frac{1331}{27}{C_A}^3C_F - \frac{484}{9}{C_A}^2C_FT_Fn_f + \frac{176}{9}C_AC_F{T_F}^2{n_f}^2\right.\\
&\quad \left. - \frac{64}{27}C_F{T_F}^3{n_f}^3\right).
\end{aligned}
\tag{106}
$$

$$
\begin{aligned}
Z_5^{(1)} &= 4C_F,\\
Z_5^{(2)} &= \frac{107}{9}C_AC_F - 22{C_F}^2 - \frac{4}{9}C_FT_Fn_f,\\
Z_5^{(3)} &= {C_A}^2C_F\left(\frac{2147}{27} - 56\zeta_3\right) + C_A{C_F}^2\left(-\frac{5834}{27} + 160\zeta_3\right) + {C_F}^3\left(\frac{370}{3} - 96\zeta_3\right)\\
&\quad + C_AC_FT_Fn_f\left(-\frac{712}{81} - \frac{64}{3}\zeta_3\right) + {C_F}^2T_Fn_f\left(\frac{124}{27} + \frac{64}{3}\zeta_3\right) - \frac{208}{81}C_F{T_F}^2{n_f}^2,\\
Z_5^{(4)} &= {C_A}^3C_F\left(\frac{324575}{648} - \frac{10498}{27}\zeta_3 + 231\zeta_4 + \frac{4120}{3}\zeta_5\right) + {C_A}^2{C_F}^2\left(-\frac{10619}{6} + 1570\zeta_3\right.\\
&\quad \left. - 660\zeta_4 - \frac{17020}{3}\zeta_5\right) + C_A{C_F}^3\left(\frac{232949}{108} - \frac{3332}{3}\zeta_3 + 396\zeta_4 + 6760\zeta_5\right)\\
&\quad + {C_F}^4\left(-\frac{1553}{2} - 564\zeta_3 - 1840\zeta_5\right) + \frac{d_F^{abcd}d_A^{abcd}}{N_R}\left(\frac{16}{3} - 760\zeta_3 - 960\zeta_5\right)
\end{aligned}
$$

$$
\begin{aligned}
&+ {C_A}^2 C_F T_F n_f \left(-\frac{18841}{162} - \frac{2236}{9}\zeta_3 + 4\zeta_4 + \frac{400}{3}\zeta_5 \right) + C_A {C_F}^2 T_F n_f \left(\frac{3410}{81} \right. \\
&\left. + \frac{2624}{9}\zeta_3 + 152\zeta_4 + \frac{80}{3}\zeta_5 \right) + {C_F}^3 T_F n_f \left(\frac{1700}{27} - \frac{232}{3}\zeta_3 - 144\zeta_4 - 160\zeta_5 \right) \\
&+ \frac{d_F^{abcd} d_F^{abcd}}{N_R} n_f \left(\frac{304}{3} - 64\zeta_3 \right) + C_A C_F {T_F}^2 {n_f}^2 \left(-\frac{146}{27} + \frac{352}{9}\zeta_3 - 32\zeta_4 \right) \\
&+ {C_F}^2 {T_F}^2 {n_f}^2 \left(\frac{2876}{81} - \frac{352}{9}\zeta_3 + 32\zeta_4 \right) + C_F {T_F}^3 {n_f}^3 \left(-\frac{40}{9} + \frac{128}{27}\zeta_3 \right). \qquad (107)
\end{aligned}
$$

We have verified the correctness of these two quantities, by verifying fermion number conservation ($\gamma^-_{\mathrm{NS}}(N=1)=0$), and by confirming the a_s^4 contribution to the Gross-Llewellyn-Smith (GLS) sum rule with [176].

4.4 CHAPTER CONCLUSION

In this chapter we have computed two classes of four-loop objects.

First, we have computed the finite pieces of all the QCD propagators and vertices with one vanishing momentum with generic colour group exactly in terms of master integrals. The results of these calculations can be used to convert quantities such as the beta function from $\overline{\mathrm{MS}}$ to any momentum subtraction scheme with a nullified momentum (see section 6.5).

Second, we have computed Mellin moments of four-loop splitting functions and coefficient functions. These are used as basic ingredients for collision processes, such as Higgs production [81]. We have computed Mellin moments $N=2,4,6$ for the non-singlet case and $N=2,4$ for the singlet case. Additionally, we have calculated $N=1,3,5$ of vector-axial interference F_3 [8]. By computing to $N=40$ and beyond, we have reconstructed the all-N n_f^2 contribution to the four-loop non-singlet splitting function and the n_f^3 contribution to the four-loop singlet splitting function [5].

Using the OPE method, we have computed up to $N=16$ for the non-singlet splitting function. For the large-n_c limit, we have computed up to $N=19$ [115]. This allowed for an all-N reconstruction and yielded a new term to the four-loop planar cusp anomalous dimension.

4.4.1 *Findings and main conclusion*

We have computed the complete finite piece of the four-loop propagators and vertices and four-loop higher Mellin moments, using the FORCER program. So far, other currently existing programs were unable to calculate these objects. Thus, these results serve as valuable contributions to the field of high precision calculations. Moreover, we may also conclude that the effectiveness of FORCER has given an adequate and sufficient answer to **RQ2**.

4

4.4.2 *Future research*

A first goal for future research is to compute the finite pieces of propagators and vertices at five loops. However, this is a formidable challenge. So far, most methods used for computations at five loops use Infrared Rearrangement (IRR), which modifies the finite terms. A direct computation would require a five-loop Forcer equivalent.

A second topic for future research is to compute higher Mellin moments. Calculating Mellin moments using the optical theorem method becomes quite hard for P_{gg} after $N = 4$. Due to its scaling behaviour, the OPE method is promising to compute more moments of the singlet case. An approximation of the x-space four-loop splitting functions derived from these future results will improve the predictions for three-loop Higgs production [81, 82, 155].